



Research article

Solar photovoltaic program helps turn deserts green in China: Evidence from satellite monitoring

Zilong Xia^{a,b}, Yingjie Li^{c,d}, Wei Zhang^{a,b}, Ruishan Chen^e, Shanchuan Guo^{a,b}, Peng Zhang^{a,b}, Peijun Du^{a,b,*}

^a Jiangsu Provincial Key Laboratory of Geographic Information Science and Technology, Key Laboratory for Land Satellite Remote Sensing Applications of Ministry of Natural Resources, School of Geography and Ocean Science, Nanjing University, Nanjing, Jiangsu, 210023, China

^b Jiangsu Center for Collaborative Innovation in Geographical Information Resource Development and Application, Nanjing, Jiangsu, 210023, China

^c Center for Systems Integration and Sustainability, Department of Fisheries and Wildlife, Michigan State University, East Lansing, MI, 48823, USA

^d Environmental Science and Policy Program, Michigan State University, East Lansing, MI, 48823, USA

^e School of Design, Shanghai Jiaotong University, Shanghai, 200241, China



ARTICLE INFO

Keywords:

Solar energy
CCDC-SMA
Fractional vegetation cover
Time series analysis
Landsat

ABSTRACT

Solar energy is considered one of the key solutions to the growing demand for energy and to reducing greenhouse gas emissions. Thanks to the relatively low cost of land use for solar energy and high power generation potential, a large number of photovoltaic (PV) power stations have been established in desert areas around the world. Despite the contribution to easing the energy crisis and combating climate change, large-scale construction and operation of PV power stations can change the land cover and affect the environment. However, few studies have focused on these special land cover changes, especially vegetation cover changes, which hinders understanding the effects of the extensive development of solar energy. Here, we used Continuous Change Detection and Classification - Spectral Mixture Analysis (CCDC-SMA) based on Landsat images to monitor changes in vegetation abundance before and after the PV power stations deployment. To reduce the interference of PV shading on vegetation abundance estimation, we improved the vegetation (VG) fraction from SMA and developed the Photovoltaics-Adjusted Vegetation (PAVG) fraction for vegetation abundance measurements in PV power stations. Results show that PV power stations in China's 12 biggest deserts expanded from 0 to 102.56 km² from 2011 to 2018, mainly distributed in the central part of north China. The desert vegetation in the deployment area of PV power stations presented a significant greening trend. Compared to 2010, the greening area reached 30.80 km², accounting for 30% of the total area of PV power stations. Overall, the large-scale deployment of PV power stations has promoted desert greening, primarily due to government-led Photovoltaic Desert Control Projects and favorable climatic change. This study shows the great benefits of PV power stations in combating desertification and improving people's welfare, which bring sustainable economic, ecological and social prosperity in sandy ecosystems.

Credit author statement

Zilong Xia: Conceptualization, Methodology, Writing – original draft, Visualization. Yingjie Li: Conceptualization, Writing – review & editing. Wei Zhang: Methodology, Writing – review & editing. Ruishan Chen: Conceptualization, Writing – review & editing. Shanchuan Guo: Writing – review & editing. Peng Zhang: Writing – review & editing. Peijun Du: Conceptualization, Methodology, Writing – review & editing, Supervision.

1. Introduction

Deserts account for 17% of the world's land area, mainly distributed in Asia and Africa (Cherlet et al., 2018; Durant et al., 2012). With the desertification caused by climate change and population growth, deserts have continued to expand in recent decades (Huang et al., 2016; Reynolds et al., 2007). The harsh environmental conditions of the desert seriously affect social-economic development (Adeel et al., 2005). As renewable energy development is accelerating globally, more and more

* Corresponding author. Jiangsu Provincial Key Laboratory of Geographic Information Science and Technology, Key Laboratory for Land Satellite Remote Sensing Applications of Ministry of Natural Resources, School of Geography and Ocean Science, Nanjing University, Nanjing, Jiangsu, 210023, China.

E-mail address: peijun@nju.edu.cn (P. Du).

<https://doi.org/10.1016/j.jenvman.2022.116338>

Received 27 June 2022; Received in revised form 28 August 2022; Accepted 18 September 2022

Available online 5 October 2022

0301-4797/© 2022 Elsevier Ltd. All rights reserved.

PV power stations are built in desert areas to meet the growing demand for sustainable energy (Kruitwagen et al., 2021; Li et al., 2018). Deserts are becoming the ideal places for constructing photovoltaic (PV) power stations, due to sufficient light conditions and broadly available land resources (Tanner et al., 2020). Apart from croplands, deserts are the most deployed areas for PV power stations worldwide by 2018 (Kruitwagen et al., 2021).

The deployment of PV power stations requires large amounts of land to accommodate solar arrays, roads, and transmission corridors, which will cause large-scale land conversion in desert areas (Edalat and Stephen, 2017; Lovich and Ennen, 2011). Vegetation coverage and inherent biological soil crusts will be disturbed during the construction process, causing increased desertification and biodiversity reduction (Grodsky and Hernandez, 2020; Scarrow, 2020; Wu et al., 2014a). After construction, PV panels block solar radiation and rainfall. The redistributed precipitation and light gradients that shift with the movement of the sun alter the carbon cycling, soil water retention, soil erosion and ecosystem energy balance below the PV panels (Tanner et al., 2020; Wu et al., 2022). Field surveys have shown that the PV panels can help maintain high soil moisture levels and relieve heat stress by adjusting the air and ground temperature, which accelerate vegetation recovery progress in arid areas (Liu et al., 2019; Marrou et al., 2013). However, vegetation recovery from PV deployment may vary across regions because of environmental heterogeneity, PV site preparation methods, and solar technology (Tanner et al., 2020). At the macro level, there is still a lack of understanding and evidence of vegetation changes in desert areas resulting from large-scale PV panel deployment, partly because large-scale field surveys can be costly and time-consuming.

Satellite remote sensing has long been instrumental in revealing both spatial and temporal vegetation patterns (Kattenborn et al., 2021). Vegetation indices, such as Normalized Vegetation Difference Index (NDVI), have been extensively used to monitor the dynamics of vegetation. For example, Potter (2016) calculated the NDVI time series using 30 consecutive years of Landsat satellite image data to quantify and characterize the vegetation canopy density changes of PV power stations across the Lower Colorado Desert region (Potter, 2016). However, influenced by factors like the soil brightness, color and texture, NDVI is inadequate in providing accurate estimates of shrubland cover in arid areas and limited utility in arid ecosystems (Dawelbait and Morari, 2012). Compared to vegetation indices, physically-based approaches, such as Spectral Mixture Analysis (SMA) utilizes information from all spectral bands and improves estimates of the fractional cover of vegetation, especially in arid areas where vegetation is sparse and vegetation indices are affected by soil color (Elmore et al., 2000). In addition, since the result from SMA is physically meaningful, its interpretation is straightforward and linked to the underlying processes (Lewńska et al., 2020). Edalat and Stephen (2017) applied SMA to analyze the land-cover change caused by establishing two PV power stations in Nevada (Edalat and Stephen, 2017). Compared to the large-scale power stations deployed in desert areas, analysis at small scales (one or two utility-scale PV power stations) in these studies can be limited and not sufficient to reveal vegetation change from satellite imagery. This research gap existed mainly because of the lack of large-scale and spatially explicit PV power stations data. While, recent advancements in mapping spatially explicit PV power stations at large scales have helped narrow the data gap (Kruitwagen et al., 2021). This advance allows us to integrate the PV spatial data with advanced satellite-derived vegetation indicators to explore vegetation changes caused by large-scale PV power stations deployment.

In this study, we took the deserts with PV power stations in China as the geographical focus. This is because numerous news has reported that PV development in deserts helped turn semi-desert green (China Daily Global, 2019; The state council of the P.R.C., 2020). But to date, there is little quantitative analysis to confirm the changes at a large scale. The objectives of this study are: (1) to detect the initial deployment date of PV power through time series analysis; (2) to quantify the vegetation

abundance within the area of PV power stations and measure the extent to which the deployment of large-scale PV power stations in deserts has contributed to vegetation recovery during 2010–2018. Here, we used Continuous Change Detection and Classification - Spectral Mixture Analysis (CCDC-SMA) model (Chen et al., 2021a) to monitor vegetation changes before and after the PV power stations deployment. We improved the vegetation (VG) fraction obtained with the SMA model and developed the Photovoltaics-Adjusted Vegetation (PAVG) fraction for vegetation abundance measurements in PV power stations. This new index can effectively reduce the interference of PV shading on vegetation abundance estimation. The analysis was implemented on Google Earth Engine (GEE) cloud-computing platform, which is highly transferable and can be easily applied to similar studies in other regions. The study revealed ecological benefits and the economic profits of deploying PV power stations in desert areas. It can help researchers and policy-makers to pay more attention to the sustainable management of large-scale PV power stations in arid ecosystems.

2. Study areas

China has vast desert areas, mainly located in the northern arid and semi-arid regions (SFA, 2011). In these areas, where ecosystems are very fragile, PV power stations are booming (Wu et al., 2014a). Here, we used the Chinese desert area mapped by Li et al. (2019) as the study area, which is established by visual interpretation of Google images (Li et al., 2019). The spatial span of the study area is large, covering 76° E–122° E and 36° N–49° N, and contains China's top 12 biggest deserts (Fig. 1): Taklamakan Desert (TakD), Gurban Tunggut Desert (GTD), Qaidam Desert (QaiD), Kumtag Desert (KumD), Badain Jaran Desert (BJD), Tengger Desert (TenD), Ulan Buh Desert (UBD), Hobq Desert (HobD), MU US Sands (MUS), Hunshandake Sands (HunS), Hulunbuir Sands (HulS), and Horqin Sands (HorS). Fig. 1 shows the spatial distribution of the major deserts. The desert area is remapped to 0.25°* 0.25° for the grid area. In addition, the spatial data of PV power stations are obtained from the global database of non-residential PV solar energy installations (Kruitwagen et al., 2021).

3. Methods and dataset

In order to analyze the vegetation changes before and after PV power stations deployment, it is important to determine the deployment time and extract vegetation information of PV power stations from Landsat time series imagery. The major procedure performed in our study comprised three steps (Fig. 2). The first step is image pre-processing. The second step is to obtain PV and vegetation information by running the CCDC-SMA model, including two sub-parts: 1) The development of five fraction images from Landsat images using SMA model, including the PAVG fraction; 2) The use of CCDC algorithm in monitoring the land cover changes to further determine the PV deployment date. The third step is analyzing the vegetation change before and after the PV power stations deployment.

3.1. Data collection and preprocessing

Surface reflectance data of Landsat-7 Enhanced Thematic Mapper Plus (ETM+) and Landsat-8 Operational Land Imager (OLI) were collected and integrated from Google Earth Engine (GEE). All available Landsat-7 and Landsat-8 Surface Reflectance images were atmospherically corrected and archived in GEE as the "LANDSAT/LE07/C01/T1_SR" and "LANDSAT/LC08/C01/T1_SR" dataset. A total of 8710 Landsat images were used in this study from 2010 to 2021, including 2162 Landsat-7 ETM+ images and 6548 Landsat-8 OLI images. We used the Quality Assessment band to detect and mask clouds and shadows and applied the USGS Landsat-7 Phase-2 Gap filling protocol (More details at <https://www.usgs.gov/media/files/landsat-7-slc-gap-filled-products-phase-two-methodology>) to fill the gaps in the Landsat-7 SLC-off

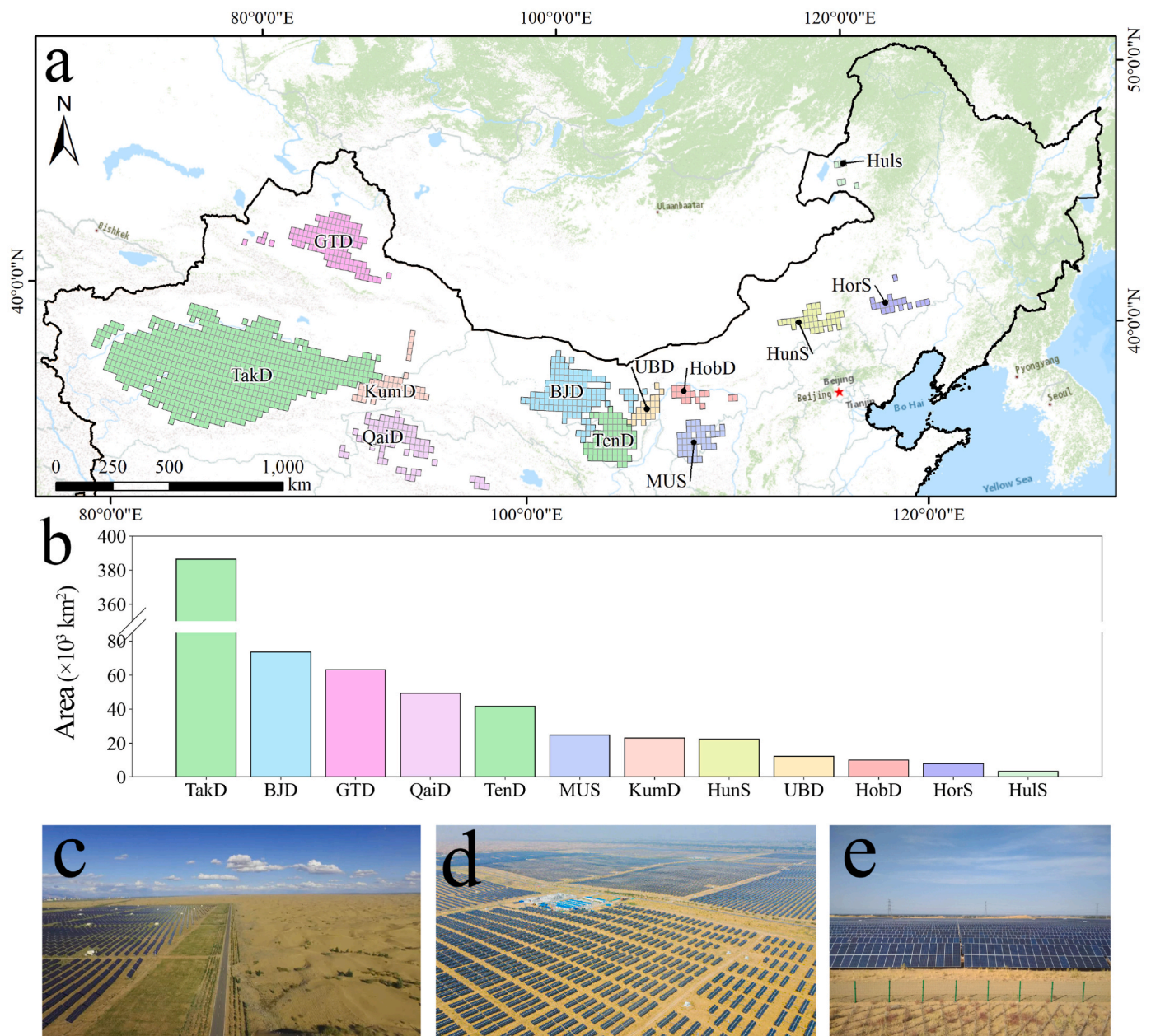


Fig. 1. Spatial distribution (a) and area (b) of large deserts in China, PV power stations located in various desert areas (c–e). Image source: <http://news.hsw.cn/system/2021/12/23/1410219.shtml>, <https://www.sohu.com/picture/418386974>, <https://www.meipian.cn/1rxa6a11>.

images. In addition, the spatial data of PV power stations in the study area were extracted from the global PV solar energy facility footprint dataset (Kruitwagen et al., 2021) and reviewed through visual interpretation to delete PV power stations misclassified.

3.2. Fractional mapping using LSMA

Among the commonly used SMA models, the Linear Spectral Mixture Analysis (LSMA) model was used to calculate the fraction of endmembers, which is easy to use and performs well in the previous study related to PV power stations (Edalat and Stephen, 2017). When relatively few endmembers are required to describe the surface composition and field data is limited, LSMA is an appropriate choice (Vermeulen et al., 2021).

Selecting appropriate endmembers is the key to successful unmixing models (Elmore et al., 2000). The PV power station is mainly composed of fixed PV panels, and the spacing between PV panels is generally less than 10 m. Considering that the spatial resolution of Landsat images is

only 30 m, each pixel is a mixture of PV panels, soil, vegetation and shadows (Edalat and Stephen, 2017). Consistent with the previous study (Edalat and Stephen, 2017), four typical endmembers applicable to PV power stations are used in desert areas, including high albedo (HA), low albedo (LA), vegetation (VG), and shadow (SH). HA represents sandy ground that reflects most of the light in this study, while LA is defined as PV panels that absorb most light. The reference image was created using the median reflectance from June to September in 2018 and principal component analysis (PCA) was used to reduce the spectral dimensionality of the image.

The potential endmembers were selected from the scatter plots of the former three PCA components (Fig. S1). The endmembers tend to choose the representative pixels nearest to the apexes of the scatter plots and the types of the pixels at the apexes were determined by linking the pixels back to the image-feature space (Edalat and Stephen, 2017; Wang et al., 2012). Different from other endmembers, the LA endmember was selected in Landsat imagery and high-resolution imagery. We selected

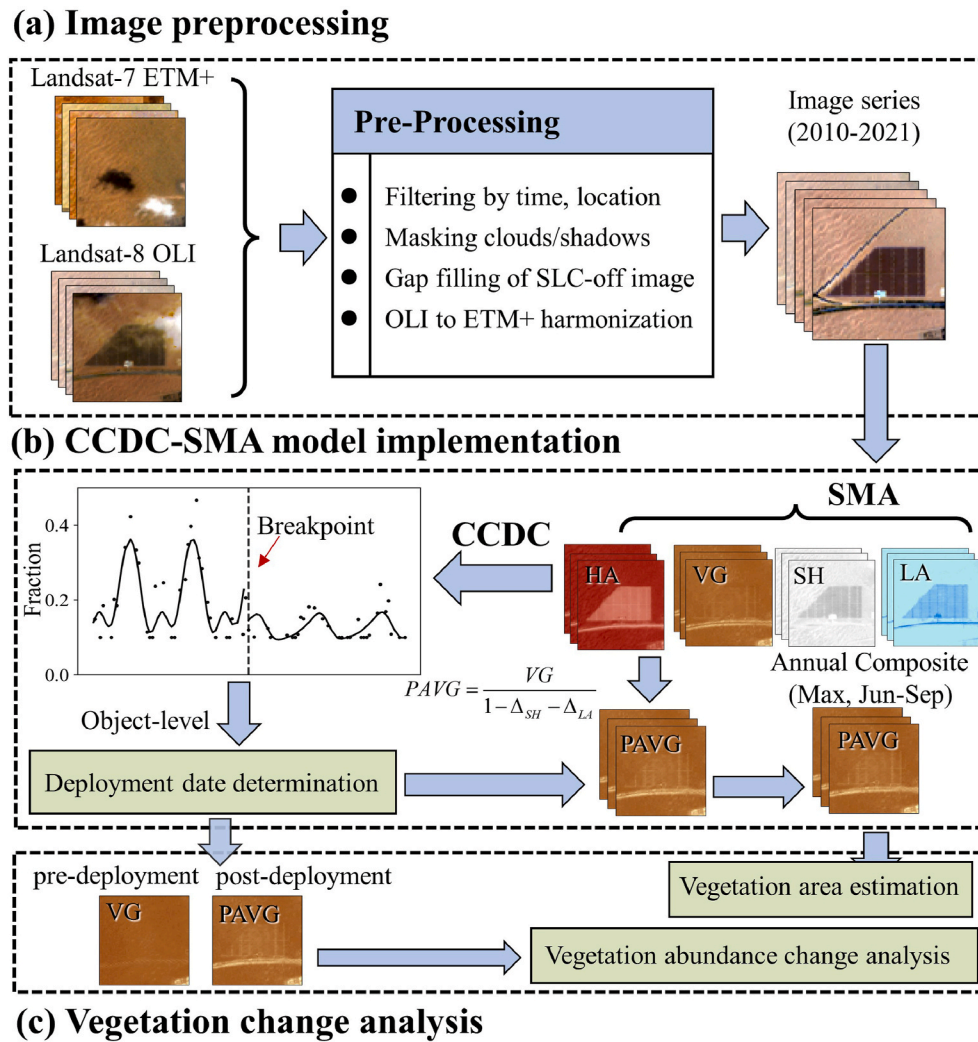


Fig. 2. Flowchart of methodology. (HA: high albedo, VG: vegetation, SH: shadow, LA: low albedo, PAVG: Photovoltaics-Adjusted Vegetation).

more than 20 candidate pixels from a large flat-roof PV facility, and took the mean of the reflectance of candidate pixels as the reflectance of final LA endmember. Fig. S1(a) shows the location of the LA endmember in the scatter plots of the first three PCA components. The LA endmember is located at the edge of the scatter plots, indicating that it is not easily confused with other endmembers. In addition, the shadow endmember was assigned to zero reflectance at all wavelengths (Chen et al., 2021a). Since the spectral features of endmembers were obtained from Landsat-8, we further harmonized Landsat-7 data to Landsat-8 data using a statistical transformation function to avoid differences in the spectral response due to sensor specifications (Roy et al., 2016). The LSMA process was implemented in GEE, and the output fractions are constrained to be non-negative and summed to one. The root mean square error (RMSE) was used to assess the model's accuracy.

3.3. Photovoltaics-Adjusted Vegetation (PAVG) fraction

Because the PV panels are usually placed at a certain angle (about 35° in desert areas of northern China) and supported by brackets, the PV panels and shadows (uniformly denoted as panel shading) would hinder the remote sensing observation of the underlying surface. In addition, field observations from several PV power stations in desert areas indicate that panel shading does not significantly affect the vegetation abundance of sandy ecosystems (Tanner et al., 2020). Therefore, we inferred that the VG fraction from SMA ignores the vegetation

abundance in areas affected by panel shading within the pixel, thus underestimating the true VG abundance in PV power stations. To reduce the interference caused by panel shading, we created a Photovoltaics-Adjusted Vegetation (PAVG) fraction, computed by the fraction images obtained with SMA model. Taking the shade-normalized Green Vegetation fraction as a reference (Souza et al., 2005), we renormalized the VG fraction by subtracting the increased LA and SH fractions after the PV power stations deployment from the denominator. The PAVG fraction represents the true vegetation abundance after the PV deployment within a pixel.

$$PAVG = \frac{VG}{1 - \Delta_{SH} - \Delta_{LA}} \quad (1)$$

Where Δ_{SH} and Δ_{LA} denote the difference of SH and LA fractions for pre-deployment and post-deployment, respectively. Here, the median of LA and SH fractions from June to September in 2010 were used as the reference values for pre-deployment. This date is sufficiently old to ensure that all PV power stations are deployed after that. Using images from June to September reduces the interference of seasonal variability (e.g. snow).

3.4. Accuracy assessment of vegetation abundances

Accuracy assessments of VG and PAVG results were conducted using the reference vegetation fractional cover information derived by visual

interpretation of very high-resolution (VHR) images. To generate the reference dataset, a total of 100 Landsat pixels (size 30×30 m) were randomly selected and then split into a 10×10 grid of 100 sample cells each. The percentages of the vegetation cover for the pixel sample were calculated through visual interpretation of the VHR images as shown in Fig. S2. These values were used as the reference to evaluate the vegetation abundances from SMA. Landsat images used in the evaluation process are derived from observations nearest to the VHR acquisition dates.

3.5. Continuous Change Detection and Classification for PV power stations

To monitor land cover changes caused by the PV power stations deployment, the time series of all endmember fractions were used to run the Continuous Change Detection and Classification (CCDC) algorithm (Zhu and Woodcock, 2014). The CCDC algorithm uses harmonic regression to predict future observations based on available observations. When new observations deviate from the predicted observations for a certain number, a break is marked and a new regression model is estimated.

Prior to the deployment of PV power stations, there was almost no significant land-use change in the desert area due to less human activity. Since the fraction of endmembers usually changes significantly with the deployment of PV power stations. The breaks in CCDC-SMA models are usually interpreted as the deployment time of PV power stations at pixel scale. We used all the fraction of endmembers as the inputs to the CCDC algorithm and limited the number of breaks. This helps reduce noise from other land cover and land use changes (such as dune movement). For each PV power station, we calculated the mode value of the deployment time for the pixels inside the PV power station and counted it as the deployment time of the PV power station (Time unit: Year), which also reduces estimation errors at the pixel scale.

In the CCDC algorithm, the number of continuous observations that determines the break is set to 6. After repeated tests, we believed that 6 was an appropriate threshold to determine the deployment time of all PV power stations. To test the accuracy of the estimated results of PV power stations deployment time, manual interpretation was used for all the PV power stations from the whole study area and 107 PV power stations were assessed in the accuracy validation. The actual deployment time was extracted by visual interpretation of time-series images. A very small percentage of PV power stations have a long construction period and are not limited to one year, leading to some uncertainty in the statistical results.

3.6. Vegetation area estimation and abundance change analysis

The ground cover area of different land cover types can be estimated with the abundances after spectral unmixing (Chen et al., 2021b). Thus, the PAVG fraction of each pixel multiplied by the corresponding pixel area was used to calculate the vegetation area at each pixel:

$$S_{veg} = PAVG_{max} \times S_{pixel} \quad (2)$$

where S_{veg} and S_{pixel} denote the vegetation area and the corresponding pixel area, respectively. $PAVG_{max}$ is the maximum value of PAVG fractions from June to September.

Abundance change analysis was used to provide information on vegetation gain and loss, and to further identify the degradation and greening of desert vegetation after the PV power stations deployment. After the PV power station deployment, we used the difference between VG images in 2010 and PAVG images to analyze vegetation abundance changes. Both images are composites using the maximum value from June to September. The difference between the abundance and actual vegetation cover is generally less than 0.15 (Lu et al., 2011; Wu and Murray, 2003), which is also applicable in this study after visual

interpretation test. Thus, we used 0.15 as the non-change threshold and defined three types as follows:

Vegetation degradation: $0.15 \leq p_{diff} \leq 1.0$

Non-change: $-0.15 < p_{diff} < 0.15$

Vegetation greening: $-1.0 \leq p_{diff} \leq -0.15$ where p_{diff} was defined as the difference between VG images in 2010 and PAVG images after the PV power stations deployment.

4. Results and analysis

4.1. Performance evaluation of the method

Fig. S3 shows the RMSEs of the LSMA model (the reflectance is scaled up by 10,000), which were calculated using the median reflectance from June to September in selected years. The average RMSEs for all years did not exceed 125, which was relatively low and showed good consistency over time (Fig. S3). Taking the results of 2018 as an example (Fig. S3(a)), higher RMSEs mainly occurred in the western desert area (TakD), while the other deserts, especially the central deserts, had low RMSE, generally less than 200. The high RMSEs are due to the fact that a fixed number of endmembers may not sufficiently deal with complex land cover compositions (Deng and Wu, 2016). The land cover at the edge of TakD is more inclined to saline-alkali land than the sandy ground, deviating from the four endmembers defined in this study. Similarly, the impervious surface is not included in the four endmembers, and can also explain the high RMSEs of impervious surface facilities inside PV power stations (Fig. S3(b)). The black area in Fig. S3(b) is the impervious water surface facilities of PV power stations (e.g. substations).

4.2. Analysis of endmember fractions and validation of fractional vegetation cover

Fig. 3 shows an example of spectral unmixing of a PV power station. Compared to the surrounding desert areas, PV power stations have high fractions of LA and SH, and low fraction of HA (Fig. 3b, e, f). In Fig. 3c, the shelterbelt is planted around the PV power station, which results in a high VG fraction at the edge of the PV power station. Compared with the original VG fraction image, the vegetation abundance of the PV power station is enhanced in the PAVG fraction image (Fig. 3f).

The quantitative relationship between two fractions (VG and PAVG) and the reference dataset is shown in Fig. S2. As expected, there is a significantly positive linear correlation between two fractions and the reference data. We found the correlation performs better for PAVG fraction than VG fraction. For PAVG fraction, we observed a consistently high agreement close to the 1:1 line with an RMSE of 0.06, while VG fraction generally underestimated vegetation cover in the PV power stations. It indicates that the PAVG fraction obtained after VG fraction correction can effectively reduce the error caused by PV shading, and ensure the consistency of vegetation cover estimation before and after the PV power station deployment.

4.3. Rapid expansion of PV power stations in China's desert areas

The deployment sites of PV power stations in desert areas can be divided into: vegetation-covered areas and non-vegetation-covered areas. Before the PV power stations deployment, the soils usually need to be graded, resulting in vegetation removal (Hernandez et al., 2014). Fig. S4 shows an example of a vegetation degradation event caused by the deployment of PV power stations. The timing of the start and completion of PV panel installation at the sample sites was derived from visual identification of the Landsat time-series imagery. The original dominant land cover type at this sample site was shrubland and sandy ground, with relatively high VG, SH, and HA fractions. After the PV power station deployment, the HA and VG fractions decreased, and the LA fraction increased significantly. The SH fraction varied less because the shrubland has a high SH fraction before.

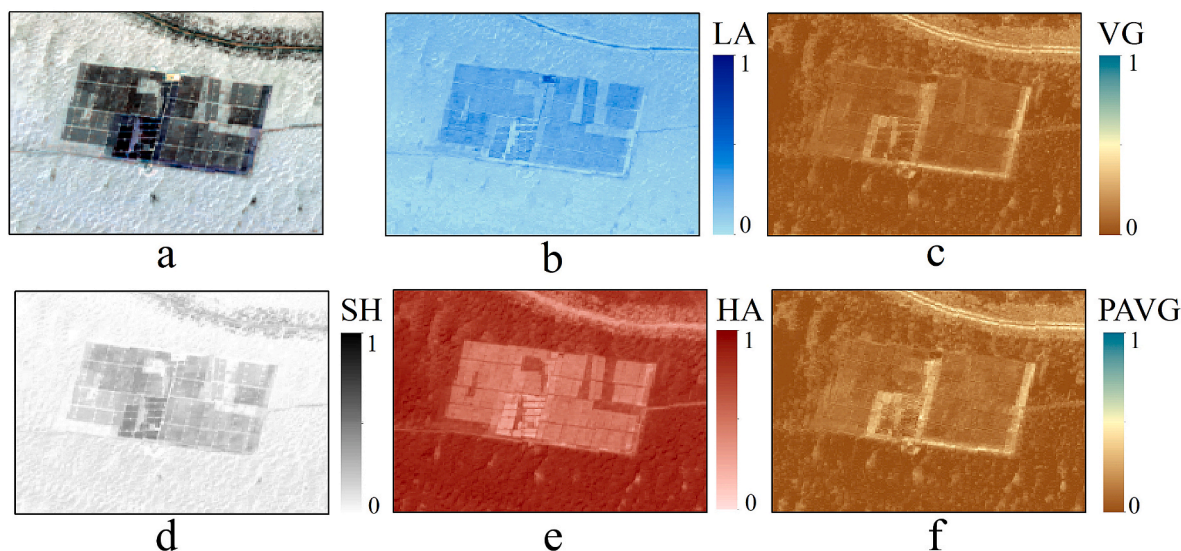


Fig. 3. An example of spectral unmixing of a PV power station in 2018: Landsat-8 image (red-green-blue) (a); Fraction of LA (b); Fraction of VG (c); Fraction of SH (d); Fraction of HA (e); Fraction of PAVG (f).. (For interpretation of the references to color in this figure legend, the reader is referred to the Web version of this article.)

In contrast, Fig. S5 shows an example of a significant increase in vegetation abundance after the PV power stations deployment. The original land cover type of the sample site was sandy ground without any vegetation. Before the PV power station deployment, the VG fraction was close to 0, and the HA fraction was very high. After deployment, the SH and LA fractions increased significantly, and the HA fraction decreased. The VG fraction also increased slightly, while the PAVG fraction increased more. In addition, the LA fraction and SH fraction of the two sample sites fluctuated greatly after deployment, which may be caused by periodic variation of the solar altitude angle.

We further identified the deployment years of all PV power stations by using the breaks in the CCDC-SMA model. The results show that China began deploying PV power stations in desert areas as early as 2011. Validation of deployment years showed that 81 of 107 PV power stations (78%) had the same interpreted deployment year as the prediction (see Fig. S6). The deployment year mean error was -0.27 years with a standard deviation of 0.52 years. The total PV power stations area increased continuously over the next eight years with an overall rate of 17 km²/year, from 0.05 km² in 2011 to 102.56 km² in 2018 (see Fig. 4). The largest gain occurred in 2016 (30.69 km²). The total area of PV power stations was unevenly distributed across space. In 2018, MUS had the largest area of PV power stations (30.80 km², 30.0%), followed by TenD (29.50 km², 28.8%), UBD (11.33 km², 11.0%) and HobD (8.14 km², 8.0%). Compared with other deserts, these four deserts are located in the central part of north China, and the surrounding areas have a higher level of economic development. Therefore, considering the

convenience for maintenance (i.e., road density), and the availability of social infrastructure (i.e., population density), these deserts become hot spots for the deployment of PV power stations, and account for approximately 80% of the total area.

4.4. Vegetation change associated with expansion of PV power stations

With the increase in PV deployment area, the vegetation area within PV power stations increased drastically from 0.02 km² in 2011 to 25.67 km² in 2018 (Fig. 5a). The proportion of vegetation area to the total area increased from 14% in 2013 to 25% in 2018. Considering the vegetation area of PV power stations in each desert in 2018, the top three deserts are MUS (10.4 km²), TenD (5.3 km²) and UBD (3.5 km²), which are consistent with the deployment area ranking (Fig. 5b). Although the deployment area of GTD and BJD is relatively high (>4 km²), the vegetation area of GTD and BJD is very low (0.36 km² and 0.07 km² respectively), which indicates that the proportion of vegetation coverage in PV power stations in different deserts is quite different.

Overall, the greening area of all deserts is much larger than the degradation area, indicating an overall greening trend of desert vegetation after the PV power stations deployment. From 2011 to 2018, the greening area within the range of PV power stations increased to 30.8 km² substantially, with the largest greening area in 2016 (31.9 km²). For most deserts, the degradation area is negligible compared to the greening area. However, due to the lack of imagery information in some areas caused by summer cloud cover, the greening area in 2017

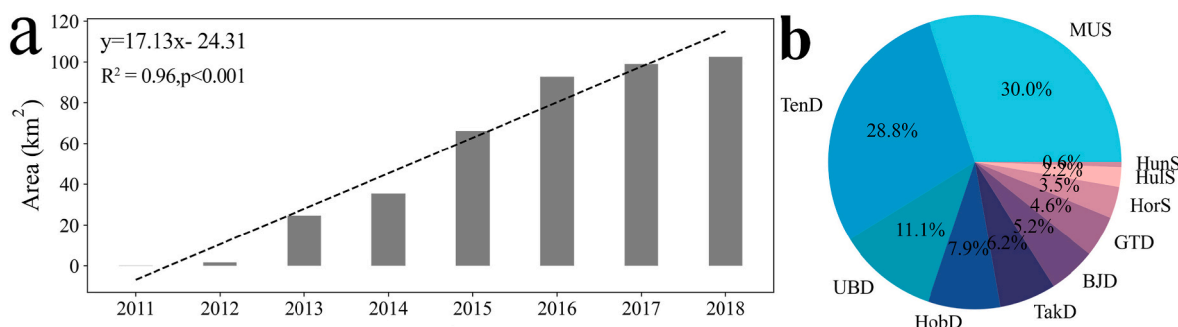


Fig. 4. Total areal changes of PV power stations in desert areas from 2011 to 2018 (a), and areal proportion in 2018 by desert (b).

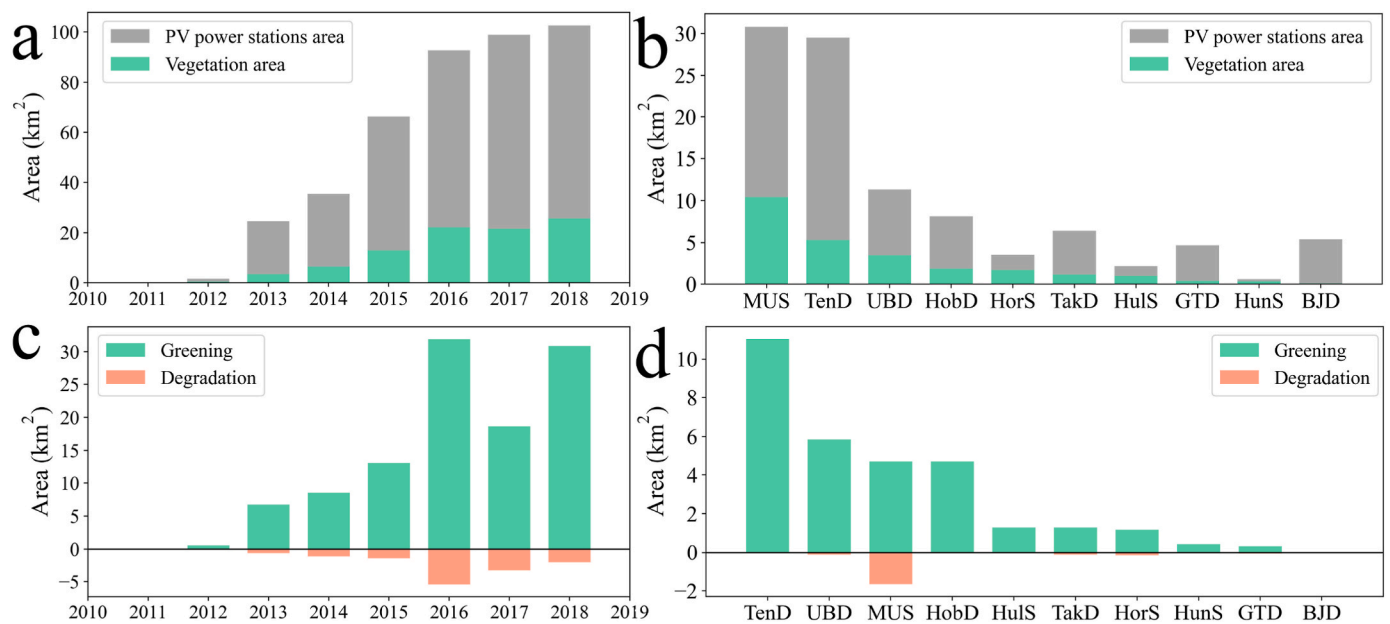


Fig. 5. Temporal variation of vegetation area (a) and vegetation abundance changes of PV power stations (c); The vegetation area (b) and vegetation abundance changes (d) in different deserts.

experienced a brief and substantial decline. On the other hand, the degradation area gradually increased and peaked (5.4 km^2) from 2011 to 2016, and then gradually decreased, with an area of 2.1 km^2 in 2018. Fig. 5d shows the greening and degradation areas in each desert in 2018. The top three deserts with the largest greening area are TenD (11.0 km^2), UBD (5.8 km^2) and MUS (4.7 km^2). In addition, MUS has the largest degradation area, four times the total degradation area of other deserts.

5. Discussion

5.1. Driving factors for the vegetation change

Previous remote sensing studies of a few PV power stations have demonstrated that the PV power station deployment does not significantly alter desert vegetation (Edalat and Stephen, 2017; Potter, 2016). In contrast, we observed significant vegetation changes caused by the deployment of PV power stations in China's desert areas, including vegetation greening and degradation. The findings suggest the importance of conducting large-scale remote sensing observations for a comprehensive understanding of the ecological impacts of PV power stations. Fig. 6a shows the difference in average vegetation abundance before and after each PV power station deployment. We selected and exhibited two typical vegetation degradation and greening examples respectively.

Desertification is a severe ecological problem in northern China, which led to huge environmental and economic losses of about 54 billion yuan per year (Tao, 2014; Zhang et al., 1996; Zhang and Hui-singh, 2018). To improve the ecological conditions and combat desertification, the Chinese government has implemented a series of ecological construction measures, such as popularizing water-saving agriculture in sandy areas or planting shrubs and trees to improve vegetation cover (Wang et al., 2010, 2012). However, the harsh ecological environment of low soil moisture content and high evaporation makes it difficult for plants to survive on sandy land.

Some studies have shown that the deployment of PV power stations will change the regional microclimate, which can help improve the growing environment for plants in arid areas (Jiang et al., 2019; Yue et al., 2021; Wu et al., 2022). Usually, after deployment, PV power stations can effectively convert solar radiation and adjust the

thermodynamic equilibrium in deserts, helping to prevent sandstorms and reduce aeolian sandflow (Chang et al., 2016). The height of PV panels is usually greater than 2.5 m, much higher than the general sand-fixing shrubbery. Therefore, PV panels and their brackets also can act as sand barriers to help combat desertification. When PV panels are deployed on a large scale, surface roughness is greatly increased and wind speed near the soil surface is reduced efficiently (Cui et al., 2017). In addition, as the PV panels block the solar radiation received at the underlying surface, this leads to a decrease in temperature below the panels (Wu et al., 2022). The lower temperature and weaker wind erosion reduce the evapotranspiration water loss and maintain a relatively higher soil water content, mitigating environmental stress in deserts and facilitating vegetation restoration (Wu et al., 2022; Liu et al., 2019). Since dust on the PV panel surface needs to be cleaned regularly in the desert, a large amount of cleaning water can also help to further elevate soil moisture content and promote vegetation growth (Cui et al., 2017).

In recent years, the Chinese government has carried out a series of Photovoltaic Desert Control Projects, aiming to combine the efforts to develop the solar PV sector with measures to control desertification (CGTN, 2017; The state council of the P.R.C., 2019; Cui et al., 2017). The Photovoltaic Desert Control Projects mainly focus on establishing tree-shrub belts around the PV power stations and plant green economic crops or psammophytic shrubs and herbaceous plants inside the PV power stations, which can facilitate sustainable economic, ecological and social prosperity in sandy ecosystems (Liu et al., 2020; Niu, 2021). Fig. 6c shows a Photovoltaic Desert Control Project in the Hobq Desert with a significant vegetation increase.

In most deserts, the degradation area caused by the deployment of PV power stations is small, probably because the amount of vegetation in these areas is negligible before deployment. With the advancement of the Photovoltaic Desert Control Projects and the natural restoration of vegetation, the vegetation removed during the construction will also be restored later (Fig. S7). Desert vegetation degradation occurs mainly in MUS, which far exceeds the area of other deserts. Fig. 6b shows the deployment of a PV power station in MUS resulting in a significant vegetation reduction. In recent decades, large ecological restoration projects implemented by the government and favorable climatic change have promoted the growth of vegetation in MUS (Cai et al., 2020; Xu

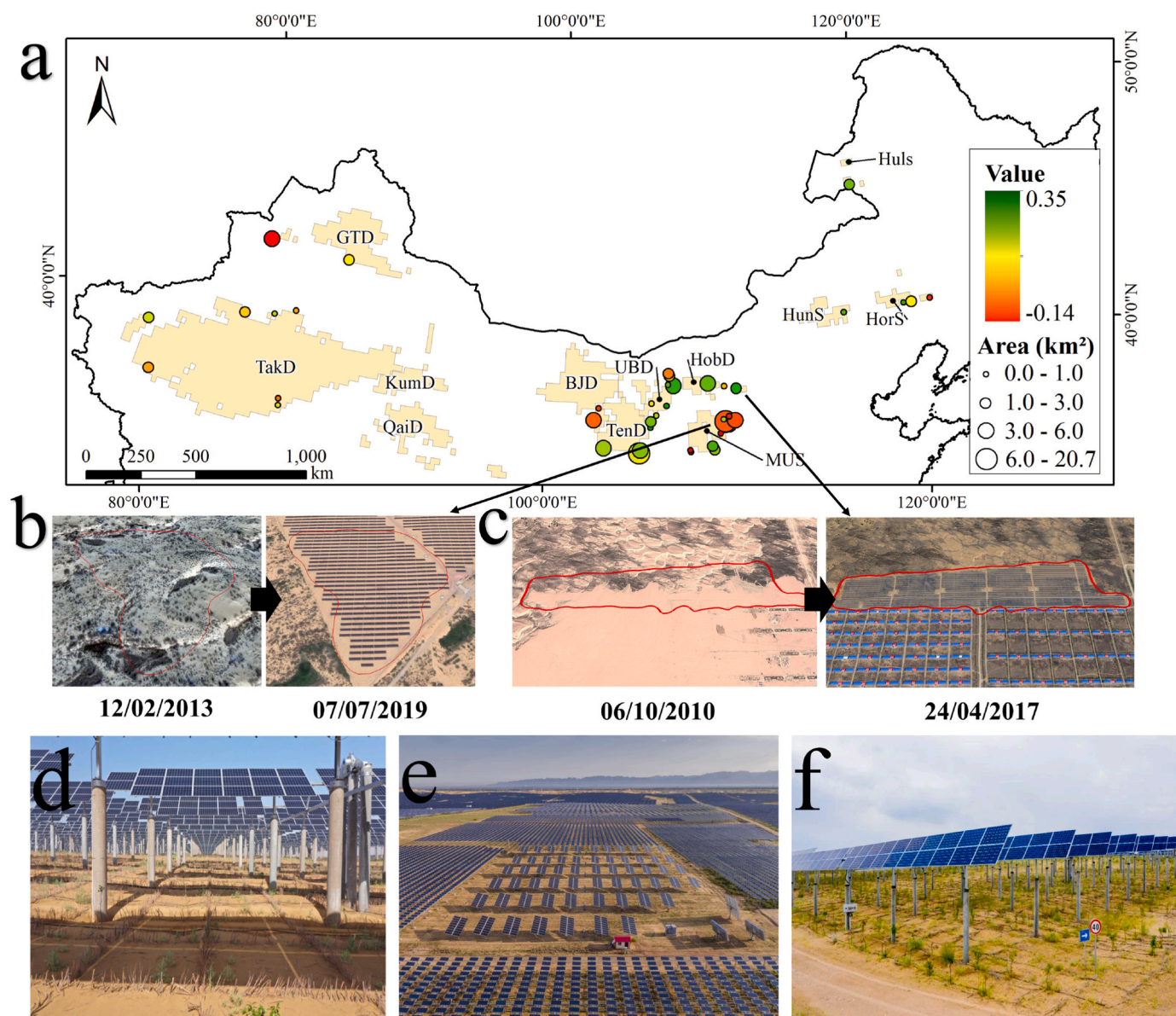


Fig. 6. The difference in average vegetation abundance before and after each PV power station deployment (a), examples of vegetation degradation (b) and greening (c). Photovoltaic desert control projects in the Hobq Desert (d–f). Image source: http://k.sina.com.cn/article_1882481753_7034645902000j4bk.html, <https://www.imsilkroad.com/news/p/105775.html>, and <https://www.sdic.com.cn/cn/rmtzx/xwzx/gzdt/yqlb/webinfo/2021/06/phone1624715576565019.htm>.

et al., 2018). The site preparation practices for the PV power stations deployment in areas with lush vegetation could make the degradation of desert vegetation more obvious. In 2019, the media reported a case of deforestation caused by a PV power station project in MUS, which was difficult to recover at a later stage (Xinhuanet, 2019), but this only happened in a few areas.

In general, the desert greening (with a significant increase in vegetation) in China from PV power station deployment is largely promoted by the policy-driven Photovoltaic Desert Control Projects. However, the human activities effects on vegetation are often superimposed on the long-term climate-driven variations. But this trend can also relate to regional climate change. Desert vegetation is sensitive to temporal changes in climatic conditions, especially precipitation (Chen et al., 2021b). Li et al. found a trend of increasing precipitation in Chinese deserts, providing favorable climatic conditions for vegetation recovery (Li et al., 2019). We used the daily rainfall dataset from CHIRPS (Funk et al., 2015) with a spatial resolution of 0.05° to calculate the average annual cumulative precipitation of PV power stations from 2011 to

2019, and found a significant increasing trend of precipitation (Fig. S8). Thus, favorable climatic conditions are also important factors in vegetation growth.

5.2. Ecological and economic benefits of solar PV programs in sandy ecosystems

In the future, China's solar PV programs will continue to expand rapidly and bring considerable ecological and economic effects in sandy ecosystems. In order to achieve carbon neutrality, China's 14th Five-Year Plan for Renewable Energy development stipulates that renewable energy needs to account for more than 50% of the increase in electricity consumption by 2025. As part of the efforts to achieve this target, the Chinese government plans to build 450 GW (GW) of solar and wind power generation capacity in the Gobi and other desert regions. The construction of large-scale PV bases in desert areas can help minimize costs and bring obvious economic benefits by making full use of unused land and bringing scale effect into play in renewable energy

supply.

Deserts account for 17% of the world's land area, and widespread desertification is affecting more than 100 countries across the world. Our research reveals that developing PV power stations in deserts might help address the desertification challenges. We found the revegetation process along with PV development is happening at large scales, which expanded previous findings at small scales (Liu et al., 2020). This fully demonstrates that PV power stations in desert areas can provide additional ecological service value in addition to electricity benefits value. The United Nations "2030 Agenda for Sustainable Development" calls on countries worldwide to address SDG 15 by "combat desertification, and halt and reverse land degradation" (Weiland et al., 2021). China has taken a leading role in developing and implementing novel PV technologies to combat desertification. The PV program in China is also proven to improve the local communities' livelihood, promoting sustainable development in desert areas (Liu et al., 2020). Compared to traditional methods for combating desertification, PV power stations can provide considerable returns in the short term, which further encourages investment in PV power station deployment. Countries experiencing serious desertification can learn from China's success and adopt a similar PV program as a sustainable land-management practice in the deserts to promote vegetation restoration and further increase the carbon sink potential of sandy ecosystems.

5.3. Limitations and future work

To the best of our knowledge, this is the first attempt to analyze vegetation changes caused by large-scale deployment of PV power stations in desert areas. The results of our research can serve as a reference for future studies on the ecological impact of deploying PV power stations. Nevertheless, there are still some limitations that should be discussed and improved.

Firstly, in the LSMA algorithm, endmembers' number and spectral characteristics are constant even at different locations and times. Especially in areas with a large heterogeneity of land cover compositions, ignoring the issues of endmember variability will increase the residual error (Li et al., 2021). To overcome this limitation and expand the study to a wider area, it is necessary to incorporate more endmembers and select more appropriate methods, such as the Multiple Endmember Spectral Mixture Analysis (MESMA) model (Roberts et al., 1998). In this study, high residual errors were found only in individual desert areas, due to the small spatial heterogeneity of desert areas.

Secondly, our study revealed the benefits of desert greening achieved by Photovoltaic Desert Control Projects. In addition, the greening of the desert may also attribute to the changes in the hydrothermal environment, or other human activities after deployment (Li et al., 2018; Wu et al., 2014a, 2022). For example, water used for regular cleaning of PV panels provides a steady water supply to revegetation. It can be seen that these direct and indirect changes can still be linked to the deployment of PV power stations (Wu et al., 2014b). Although this study cannot fully explain the process and mechanism, the increased vegetation from PV development might facilitate future work on analyzing the environmental impact of PV power stations in desert areas and the response of internal vegetation to temperature and precipitation. This can be done by distinguishing environmental impacts and anthropogenic impacts (e. g., weeding, ecological restoration, and watering from solar panel cleaning). However, due to the lack of data at the current stage, we were not able to include this analysis in this work.

Finally, we focus more on vegetation abundance in our study, while other environmental changes such as the potential risk of affecting biodiversity in sandy ecosystems by the deployment of PV power stations deserve attention but are not covered in this study due to limited data (Graham et al., 2021; Grodsky and Hernandez, 2020).

6. Conclusions

This study used CCDC-SMA and the proposed PAVG fraction to analyze vegetation changes caused by large-scale deployment of PV power stations in desert areas. The results demonstrated that PV plants in China's desert regions have expanded rapidly in recent years, reaching 102.56 km² in 2018. The desert vegetation in the deployment area of PV power stations shows a greening trend. The greening area has reached 30.8 km², which is mainly attributed to government-led Photovoltaic Desert Control Projects and favorable climatic conditions. These findings show the great benefits of PV power stations in combating desertification and help decision-makers in PV power station construction to better promote vegetation restoration and management in sandy ecosystems. As the rapid development of the PV industry brings new opportunities and challenges, more work is needed to evaluate the trade-offs between achieving multiple benefits by deploying PV power stations in desert areas.

Declaration of competing interest

The authors declare that they have no known competing financial interests or personal relationships that could have appeared to influence the work reported in this paper.

Data availability

The data that has been used is confidential.

Acknowledgments

The authors express their gratitude to Guoshuai Li from the Institute of Tibetan Plateau Research for providing the spatial data of China deserts. This study was funded by the National Natural Science Foundation of China (No. 41631176).

Appendix A. Supplementary data

Supplementary data to this article can be found online at <https://doi.org/10.1016/j.jenvman.2022.116338>.

References

- Weiland, S., Hickmann, T., Lederer, M., Marquardt, J., Schwendenhammer, S., 2021. The 2030 agenda for sustainable development: transformative change through the sustainable development goals? *Polit. Govern.* 9, 90–95.
- Adeel, Z., Safriel, U., Niemeijer, D., White, R., 2005. *Ecosystems and Human Well-Being: Desertification Synthesis*. World Resources Institute (WRI).
- Cai, D., Ge, Q., Wang, X., Liu, B., Goudie, A.S., Hu, S., 2020. Contributions of ecological programs to vegetation restoration in arid and semiarid China. *Environ. Res. Lett.* 15, 114046.
- CGTN, 2017. Model of Desert Economy: Turn the Desert Back Green Again. <https://news.cgtn.com/news/7a49444f78557a633566d54/index.html>. (Accessed 9 March 2022). accessed.
- Chang, Z., Liu, S., Zhu, S., Han, F., Zhong, S., Duan, X., 2016. Ecological functions of PV power plants in the desert and Gobi. *Journal of Resources and Ecology* 7, 130–136.
- Chen, S., Woodcock, C.E., Bullock, E.L., Arévalo, P., Torchinava, P., Peng, S., Olofsson, P., 2021a. Monitoring temperate forest degradation on Google Earth Engine using Landsat time series analysis. *Remote Sens. Environ.* 265, 112648.
- Chen, Y., Huang, X., Huang, J., Liu, S., Lu, D., Zhao, S., 2021b. Fractional monitoring of desert vegetation degradation, recovery, and greening using optimized multi-endmembers spectral mixture analysis in a dryland basin of Northwest China. *GIScience Remote Sens.* 58, 300–321.
- Cherlet, M., Hutchinson, C., Reynolds, J., Hill, J., Sommer, S., Von Maltitz, G., 2018. *World Atlas of Desertification*. Publication Office of the European Union, Luxembourg, p. 180.
- China Daily Global, 2019. Photovoltaic Park Helps Turn Semi-desert Green. http://www.chinadaily.com.cn/global/2019-09/05/content_37507950.html. (Accessed 9 March 2022). accessed.
- Cui, Y., Feng, Q., Sun, J., Xiao, J., 2017. A review of revegetation patterns of photovoltaic plant in northwest China. *Bull. Soil Water Conserv.* 37, 200–203.
- Dawelbait, M., Morari, F., 2012. Monitoring desertification in a Savannah region in Sudan using Landsat images and spectral mixture analysis. *J. Arid Environ.* 80, 45–55.

- Deng, Y., Wu, C., 2016. Development of a class-based multiple endmember spectral mixture analysis (C-MESMA) approach for analyzing urban environments. *Rem. Sens.* 8, 349.
- Durant, S.M., Pettorelli, N., Bashir, S., Woodroffe, R., Wachter, T., Ornellas, P.D., Ransom, C., Abäigar, T., Abdelgadir, M., Alqamy, H.E., Beddiaf, M., Belbachir, F., Belbachir-Bazi, A., Berbash, A.A., Beudels-Jamar, R., Boitani, L., Breitenmoser, C., Cano, M., Chardonnet, P., Collen, B., Cornforth, W.A., Cuzin, F., Gerngross, P., Haddane, B., Hadjeloum, M., Jacobson, A., Jebali, A., Lamarque, F., Mallon, D., Minkowski, K., Monfort, S., Ndoassal, B., Newby, J., Ngakoutou, B.E., Niagate, B., Purchase, G., Samaïla, S., Samna, A.K., Sillero-Zubiri, C., Soltan, A.E., Price, M.R.S., Baillie, J.E.M., 2012. Forgotten biodiversity in desert ecosystems. *Science* 336, 1379–1380.
- Edalat, M.M., Stephen, H., 2017. Effects of two utility-scale solar energy plants on land-cover patterns using SMA of Thematic Mapper data. *Renew. Sustain. Energy Rev.* 67, 1139–1152.
- Elmore, A.J., Mustard, J.F., Manning, S.J., Lobell, D.B., 2000. Quantifying vegetation change in semiarid environments: precision and accuracy of spectral mixture analysis and the normalized difference vegetation index. *Remote Sens. Environ.* 73, 87–102.
- Funk, C., Peterson, P., Landsfeld, M., Pedreros, D., Verdin, J., Shukla, S., Husak, G., Rowland, J., Harrison, L., Hoell, A., Michaelsen, J., 2015. The climate hazards infrared precipitation with stations—a new environmental record for monitoring extremes. *Sci. Data* 2, 150066.
- Graham, M., Ates, S., Melathopoulos, A.P., Moldenke, A.R., DeBano, S.J., Best, L.R., Higgins, C.W., 2021. Partial shading by solar panels delays bloom, increases floral abundance during the late-season for pollinators in a dryland, agrivoltaic ecosystem. *Sci. Rep.* 11, 7452.
- Grodsky, S.M., Hernandez, R.R., 2020. Reduced ecosystem services of desert plants from ground-mounted solar energy development. *Nat. Sustain.* 3, 1036–1043.
- Hernandez, R.R., Easter, S.B., Murphy-Mariscal, M.L., Maestre, F.T., Tavassoli, M., Allen, E.B., Barrows, C.W., Belnap, J., Ochoa-Hueso, R., Ravi, S., Allen, M.F., 2014. Environmental impacts of utility-scale solar energy. *Renew. Sustain. Energy Rev.* 29, 766–779.
- Huang, J., Yu, H., Guan, X., Wang, G., Guo, R., 2016. Accelerated dryland expansion under climate change. *Nat. Clim. Change* 6, 166–171.
- Jiang, C., Liu, J., Zhang, H., Zhang, Z., Wang, D., 2019. China's progress towards sustainable land degradation control: insights from the northwest arid regions. *Ecol. Eng.* 127, 75–87.
- Kattenborn, T., Leitloff, J., Schiefer, F., Hinz, S., 2021. Review on convolutional neural networks (CNN) in vegetation remote sensing. *ISPRS J. Photogrammetry Remote Sens.* 173, 24–49.
- Kruitwagen, L., Story, K.T., Friedrich, J., Byers, L., Skillman, S., Hepburn, C., 2021. A global inventory of photovoltaic solar energy generating units. *Nature* 598, 604–610.
- Lewnińska, K.E., Hostert, P., Buchner, J., Bleyhl, B., Radeloff, V.C., 2020. Short-term vegetation loss versus decadal degradation of grasslands in the Caucasus based on Cumulative Endmember Fractions. *Remote Sens. Environ.* 248, 111969.
- Li, Y., Kalnay, E., Motesharrei, S., Rivas, J., Kucharski, F., Kirk-Davidoff, D., Bach, E., Zeng, N., 2018. Climate model shows large-scale wind and solar farms in the Sahara increase rain and vegetation. *Science* 361, 1019.
- Li, G., Yang, H., Zhang, Y., Huang, C., Pan, X., Ma, M., Song, M., Zhao, H., 2019. More extreme precipitation in Chinese deserts from 1960 to 2018. *Earth Space Sci.* 6, 1196–1204.
- Li, K., Wang, L., Yin, D., 2021. Deriving corn and soybeans fractions with land remote-sensing satellite (system, Landsat) imagery by accounting for endmember variability on Google Earth engine. *Int. J. Rem. Sens.* 42, 4493–4513.
- Liu, Yu, Zhang, Ruiqi, Huang, Ze, et al., 2019. Solar photovoltaic panels significantly promote vegetation recovery by modifying the soil surface microhabitats in an arid sandy ecosystem. *Land Degrad. Dev.* 30, 2177–2186.
- Liu, Y., Zhang, R.-Q., Ma, X.-R., Wu, G.-L., 2020. Combined ecological and economic benefits of the solar photovoltaic industry in arid sandy ecosystems. *J. Clean. Prod.* 262, 121376.
- Lovich, J.E., Ennen, J.R., 2011. Wildlife conservation and solar energy development in the desert southwest, United States. *Bioscience* 61, 982–992.
- Lu, D., Batistella, M., Moran, E., Hetrick, S., Alves, D., Brondizio, E., 2011. Fractional forest cover mapping in the Brazilian Amazon with a combination of MODIS and TM images. *Int. J. Rem. Sens.* 32, 7131–7149.
- Marrou, H., Dufour, L., Wery, J., 2013. How does a shelter of solar panels influence water flows in a soil-crop system? *Eur. J. Agron.* 50, 38–51.
- Niu, F., 2021. Complementary sand control mode of forestry and photovoltaic industry in kubuqi desert — a case study of dalad banner. *Inner Mongolia Forestry Investigation and Design (in Chinese)* 44, 3.
- Potter, C., 2016. Landsat time series analysis of vegetation changes in solar energy development areas of the Lower Colorado Desert, southern California. *J. Geosci. Environ. Protect.* 4, 1–6.
- Reynolds, J.F., Smith, D.M.S., Lambin, E.F., Turner, B.L., Mortimore, M., Batterbury, S.P. J., Downing, T.E., Dowlatabadi, H., Fernández, R.J., Herrick, J.E., Huber-Sannwald, E., Jiang, H., Leemans, R., Lynam, T., Maestre, F.T., Ayarza, M., Walker, B., 2007. Global desertification: building a science for dryland development. *Science* 316, 847–851.
- Roberts, D.A., Gardner, M., Church, R., Ustin, S., Scheer, G., Green, R., 1998. Mapping chaparral in the Santa Monica Mountains using multiple endmember spectral mixture models. *Rem. Sens. Environ.* 65, 267–279.
- Roy, D.P., Kovalsky, V., Zhang, H.K., Vermote, E.F., Yan, L., Kumar, S.S., Egorov, A., 2016. Characterization of Landsat-7 to Landsat-8 reflective wavelength and normalized difference vegetation index continuity. *Remote Sens. Environ.* 185, 57–70.
- Scarrow, R., 2020. Solar plants versus desert plants. *Nature Plants* 6, 908–908.
- Souza, C.M., Roberts, D.A., Cochrane, M.A., 2005. Combining spectral and spatial information to map canopy damage from selective logging and forest fires. *Remote Sens. Environ.* 98, 329–343.
- Tanner, K.E., Moore-O'Leary, K.A., Parker, I.M., Pavlik, B.M., Hernandez, R.R., 2020. Simulated solar panels create altered microhabitats in desert landforms. *Ecosphere* 11, e03089.
- Tao, W., 2014. Aeolian desertification and its control in Northern China. *International Soil and Water Conservation Research* 2, 34–41.
- The State Council of the People's Republic of China (P.R.C.), 2019. Kubuqi sets good example of China's desertification control. http://english.www.gov.cn/news/photos/2019/03/15/content_281476563384560.htm. accessed 9 Mar 2022.
- The State Council of the People's Republic of China (P.R.C.), 2020. Solar park helps turn large wasteland green. http://english.www.gov.cn/news/videos/202007/01/content_WS5efc249bc6d05a0f8970679d.html. accessed 9 Mar 2022.
- The State Forestry Administration (SFA), 2011. A Bulletin of Status Quo of Desertification and Sandification in China. State Forestry Administration Beijing.
- Vermeulen, L.M., Munch, Z., Palmer, A., 2021. Fractional vegetation cover estimation in southern African rangelands using spectral mixture analysis and Google Earth Engine. *Comput. Electron. Agric.* 182, 105980.
- Wang, X.M., Zhang, C.X., Hasi, E., Dong, Z.B., 2010. Has the Three Norths Forest Shelterbelt Program solved the desertification and dust storm problems in arid and semiarid China? *J. Arid Environ.* 74, 13–22.
- Wang, T., Yan, C.Z., Song, X., Xie, J.L., 2012. Monitoring recent trends in the area of aeolian desertified land using Landsat images in China's Xinjiang region. *ISPRS J. Photogrammetry Remote Sens.* 68, 184–190.
- Wu, C., Murray, A.T., 2003. Estimating impervious surface distribution by spectral mixture analysis. *Rem. Sens. Environ.* 84, 493–505.
- Wu, Z., Hou, A., Chang, C., Huang, X., Shi, D., Wang, Z., 2014a. Environmental impacts of large-scale CSP plants in northwestern China. *Environmental science. Processes & impacts* 16, 2432–2441.
- Wu, Z., Hou, A., Chang, C., Huang, X., Shi, D., Wang, Z., 2014b. Environmental impacts of large-scale CSP plants in northwestern China. *Environ. Sci. J. Integr. Environ. Res.: Process. Impacts* 16, 2432–2441.
- Wu, C., Liu, H., Yu, Y., Zhao, W., Liu, J., Yu, H., Yetemen, O., 2022. Ecohydrological effects of photovoltaic solar farms on soil microclimates and moisture regimes in arid Northwest China: a modeling study. *Sci. Total Environ.* 802, 149946.
- Xinhuanet, 2019. The Tracking of Deforestation in Shaanxi Yulin to Build PV Power Stations. http://www.xinhuanet.com/politics/2019-12/26/c_1125392623.htm. accessed 9 Mar 2022.
- Xu, Z., Hu, R., Wang, K., Mason, J.A., Wu, S.-Y., Lu, H., 2018. Recent greening (1981–2013) in the Mu Us dune field, north-central China, and its potential causes. *Land Degrad. Dev.* 29, 1509–1520.
- Yue, S., Guo, M., Zou, P., Wu, W., Zhou, X., 2021. Effects of photovoltaic panels on soil temperature and moisture in desert areas. *Environ. Sci. Pollut. Control Ser.* 28, 17506–17518.
- Zhang, Z., Huisin, D., 2018. Combating desertification in China: monitoring, control, management and revegetation. *J. Clean. Prod.* 182, 765–775.
- Zhang, Y., Ning, D., Smil, V., 1996. An estimate of economic loss for desertification in China. *China Popul. Resour. Environ.* 6, 45–49.
- Zhu, Z., Woodcock, C.E., 2014. Continuous change detection and classification of land cover using all available Landsat data. *Remote Sens. Environ.* 144, 152–171.